

pubs.acs.org/acscatalysis Research Article

Revealing the Mechanistic Details for the Selective Deoxygenation of Carboxylic Acids over Dynamic MoO₃ Catalysts

Laura A. Gomez, Caleb Q. Bavlnka, Tianhao E. Zhang, Daniel E. Resasco, and Steven P. Crossley*



Cite This: ACS Catal. 2023, 13, 8455-8466



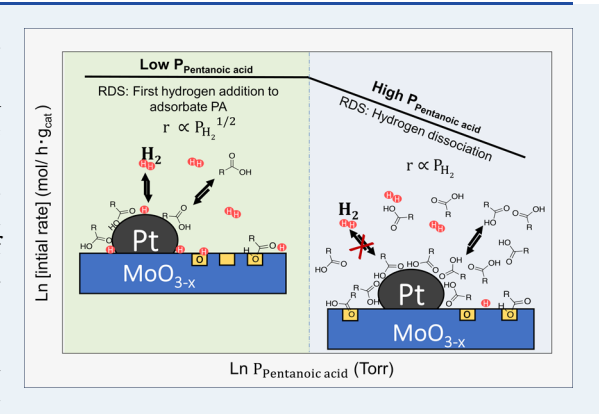
ACCESS I

Metrics & More

Article Recommendations

s Supporting Information

ABSTRACT: The selective activation of renewable carboxylic acids could enable the formation of a variety of highly valuable renewable products, including surfactants, valuable dienes, and renewable hydrogen carriers. A kinetic study is performed to enhance understanding of the selective deoxygenation of carboxylic acid on promoted MoO₃ at mild temperatures. Although several studies indicate that deoxygenation of oxygenated biomass-derived compounds on MoO₃ occurs via a reverse Mars—van Krevelen mechanism, this study suggests that the deoxygenation of pentanoic acid (PA) on an oxygen vacancy can also be explained by a Langmuir—Hinshelwood mechanism. A detailed analysis of the experimental data indicates that the incorporation of Pt on MoO₃ shifts the reaction order with respect to hydrogen from 1 to 0.5 at a low partial pressure of PA. We reveal that the rate-determining step (RDS) shifts upon the incorporation of Pt from H₂ dissociation to H addition to adsorbed acid



molecules. We further illustrate how the RDS can shift as a function of PA coverage. The inhibition effect of PA and its possible causes are discussed for both MoO_3 and 0.05 wt % Pt/MoO_3 catalysts. Here, we decouple promoter effects from the creation of highly active sites located at the Pt/MoO_3 interface. The nature of the active site involved upon Pt incorporation is also studied by separating Pt from MoO_3 at a controlled distance using carbon nanotubes as hydrogen bridges, confirming that the kinetically relevant role of Pt is to serve as a promoter of the MoO_3 .

KEYWORDS: MoO3, carboxylic acid, kinetics, mechanism, deoxygenation, hydrogen spillover

1. INTRODUCTION

The selective deoxygenation of carboxylic acids is of fundamental interest since carboxylic acids derived from biomass have been proposed to serve as precursors to high-value fuels and chemicals. ^{1–3} Selective conversion of light carboxylic acids to ethanol, ^{4,5} C-5 acids to valuable commodity chemicals, ^{6–8} and larger fatty acids to fuels and surfactants ⁹ are all important chemical transformations that rely on very active and selective catalysts. The recent emergence of the hydrogen economy has also identified these molecules as potential reversible hydrogen carriers if selectively converted to alcohols. ^{10,11} Selective deoxygenation of carboxylic acids with highly oxophilic catalysts is a promising approach toward achieving selective oxygen removal without influencing other chemical functionalities. ^{12–14}

Metal-supported oxides are known to be active and selective for the deoxygenation of biomass-derived compounds. ¹⁵ Pestman et al. showed that metal oxides with intermediate metal—oxygen bond strength are the most active and selective catalysts for the deoxygenation of carboxylic acids ⁴ without the need for sulfur addition required by traditional hydrotreating catalysts. ⁵ Prasomsri et al. showed that at low hydrogen pressures, molybdenum oxide is an effective catalyst for the

hydrodeoxygenation (HDO) of ketones and alcohols, capable of selectively breaking C–O bonds while minimizing carbon loss. $^{16-18}$ Therefore, MoO₃ is an attractive catalyst for the selective deoxygenation (SDO) of carboxylic acids.

In our recent work, we demonstrated that MoO_3 is a very selective catalyst for the deoxygenation of pentanoic acid (PA) to pentanal (PAL)¹⁹ since MoO_3 promotes C–O breaking without saturating C=C bonds or breaking C–C bonds. However, its poor ability to promote H_2 dissociation limits this selective deoxygenation. To increase MoO_3 activity, a very low loading (0.05 wt %) of Pt metal was incorporated to promote H_2 dissociation and facilitate the formation of oxygen vacancies. Similarly, several studies have shown that the incorporation of Pt on different metal oxides (TiO₂ and Fe₂O₃) drastically promotes the deoxygenation rate of acetic acid. 12,13 We showed that the addition of small loadings of Pt

Received: March 7, 2023 Revised: May 30, 2023



on MoO_3 could increase the SDO rates of PA and reduce the temperature required by 40 $^{\circ}C$ to achieve a similar SDO conversion as MoO_3 .

The interaction of a noble metal with a reducible metal oxide can generate new highly active sites at the interface that, in some cases, account for most or all of the HDO activity. 21-23 In some instances, it can be challenging to distinguish these highly active sites located at the metalsupport interface from surface-promoted effects created by hydrogen spillover from the metal.²⁴ To maximize SDO rates and design a better catalyst system, it is important to identify the active sites responsible for this chemistry. Therefore, in this study, we separated Pt from MoO₃ over a conductive carbon nanotube support to unravel its synergistic effects under reaction conditions. By doing so, the role of the oxygen vacancies can be decoupled from the unique sites created at the Pt/MoO₃ interface. Here, we prove that the role of Pt for this reaction is only to provide a constant supply of H atoms, used either as a reactant to convert PA into PAL or to regenerate oxygen vacancies on the surface.

Several studies have proposed that the deoxygenation of oxygenated compounds on metal oxides occurs via a reverse Mars—van Krevelen (MvK) mechanism. 12,13,25–28 However, our results suggest that the deoxygenation of PA occurs through a more complex mechanism, highly dependent on the local surface H concentration. To gain more insight into the mechanism, a Langmuir—Hinshelwood kinetic model is developed since it closely describes the dynamic redox chemistry that occurs at the surface for both MoO₃ and 0.05 wt % Pt/MoO₃. Herein, we reveal that upon the incorporation of Pt in MoO₃, the rate-limiting step shifts from H₂ dissociation to the first H addition to the surface-bound species. The inhibition effect of both PA and water is also discussed.

2. EXPERIMENTAL SECTION

2.1. Chemical and Catalyst Materials. All the gases ($\rm H_2$ (99.999%), He (99.999%), $\rm N_2$ (99.998%), air (ultra zero), and ethylene) used for catalyst preparation, reaction, carbon nanotube synthesis, and characterization were purchased from Airgas. Commercial molybdenum(VI) oxide, $\rm MoO_3$ (>99.5 wt %), was purchased from Alfa Aesar. Acid-washed glass beads (50–70 US sieve, Sigma) were mixed with the catalyst and packed in the reactor. Water (18 $\rm M\Omega$) was obtained from an in-house filtration system and used in this study.

For the growth of vertical multiwalled carbon nanotubes (CNTs), iron nitrate nonahydrate, cobalt nitrate hexahydrate, aluminum nitrate nonahydrate, and 2-hydroxyethyl cellulose ($M_{\rm w}\approx 1,300,000$) were used. Tungsten (1 mm, 99.94%), molybdenum (0.75 mm, 99.95%), and platinum (0.025 mm, 99.00%) wires were used for metal deposition. Aluminum conductive tape (single adhesive surface, 12.7 mm W × 16.4 m L, Ted Pella Inc.) was used to remove CNTs from the silicon wafers. The silicon wafers used as a base for growing CNTs were purchased from Wafer World, Inc. (SKU:1186). Cleaning of these wafers required isopropanol, ethanol, and acetone.

2.2. Catalyst Synthesis. 2.2.1. Supported Pt on MoO₃. The promoted molybdenum oxide (0.05 wt % Pt/MoO₃) catalysts were prepared by the incipient wetness impregnation method by using tetraammineplatinum(II) nitrate ([Pt-(NH₃)₄](NO₃)₂, 99.99%, 50% Pt, Alfa Aesar) as a Pt precursor solution. For each batch, 10 g of MoO₃ was used, and 2 mL

aqueous solution with 10 mg of Pt precursor was added dropwise to the support. Once the impregnation step was completed, the sample was dried at 80 °C for 12 h and calcined at 600 °C (ramp rate 10 °C/min) for 3 h by flowing air (100 mL/min). Commercial MoO₃ was calcined under identical conditions. Before catalytic testing, the catalyst powders were pelletized and sieved to yield 90 to 125 μ m pellets (120–170 US sieve).

2.2.2. Vertical Multiwalled Carbon Nanotube Growth. Silicon wafers were cut into 23 mm × 23 mm square pieces using a diamond scribe. The wafers were calcined in a horizontal furnace under continuous airflow (150 SCCM) at 600 °C for 2 h. Then, the wafers were ultrasonically washed in subsequent acetone, ethanol, and isopropanol solutions for 45 min each to ensure a clean surface for spin coating. A catalyst solution consisting of 1.11 wt % iron nitrate nonahydrate, 0.39 wt % cobalt nitrate hexahydrate, 1.23 wt % aluminum nitrate nonahydrate, and 0.74 wt % 2-hydroxyethyl cellulose, all with respect to water, was made. One milliliter of catalyst solution was spin-coated on each silicon wafer in a two-step process that consisted of 10 s at 500 rpm followed by 30 s at 2000 rpm. The silicon wafers were dried overnight and calcined the following day at 450 °C under continuous air flow (150 SCCM) for 1 h.

To synthesize carbon nanotubes on the silicon wafer catalyst, the samples were balanced on top of one another in a 1 inch quartz-diameter tube, ensuring that each catalyst surface was accessible to flowing gas. The vertical reactor was heated to 650 °C at 10 °C min⁻¹ under hydrogen flow (200 SCCM) and maintained at 650 °C for 30 min to ensure reduction of the catalyst. Then, nitrogen (370 SCCM) was flowed through the reactor tube and heated to a reaction temperature of 675 °C at 10 °C min⁻¹. The system was held at 675 °C for 30 min under nitrogen flow. Carbon nanotube synthesis occurred as ethylene (200 SCCM) was mixed for 20 min with the flowing nitrogen. After CNT synthesis, nitrogen was fed into the reactor until the system was cooled.

To weaken the interaction between the CNTs and the silicon wafer, the sample was calcined in air (150 SCCM) at 480 $^{\circ}$ C for 2 h. This allowed for controllable removal of the CNTs from the silicon wafer.

2.2.3. Depositing Different Catalysts on Opposite Ends of CNTs. A custom-built vacuum evaporator was used for depositing Pt and Mo onto the CNTs. To synthesize CNTs with Pt and Mo deposited on opposite ends (Pt/CNT/ MoO₃), Pt metal was deposited on the exposed end of the CNTs on the silicon wafer. Aluminum tape was then used to remove the CNTs from the silicon wafer. This flipped the orientation of the CNTs, causing the exposed end of the forest to be free of any Pt. The CNTs on aluminum tape were returned to the evaporator, and Mo was evaporated on the other end of the CNTs. The edges of the aluminum tape containing the CNT samples were removed with a razor blade to prevent contamination from any excess metal not deposited on the CNTs. The synthesized (Pt/CNT/MoO₃) samples were submerged in acetone for 45 seconds. This removed CNTs from the adhesive tape. The solution was then filtered to obtain the synthesized sample. The sample was calcined in air (150 SCCM) at 350 °C for 1 h to remove any adhesive residue from the tape. Weight percentages of all deposited metals can be found in Table S1.

2.3. Kinetic Measurements. The catalytic testing occurred in a gas-phase packed bed reactor under atmospheric

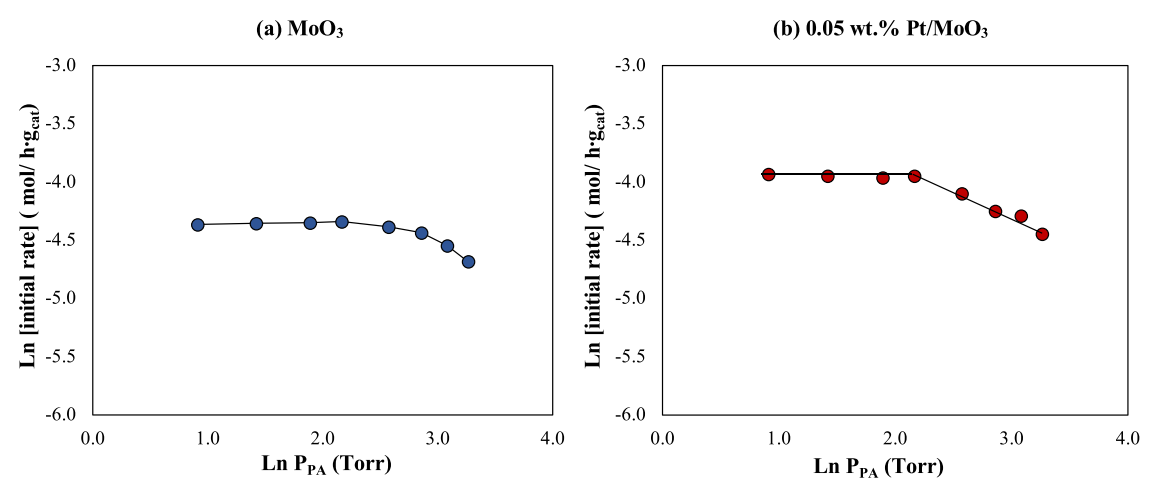


Figure 1. (a) Order of reaction with respect to PA over MoO₃. (b) Order of reaction with respect to PA using 0.05 wt % Pt/MoO₃ as a catalyst. Reaction conditions: Flow of $H_2 = 30$ mL/min, $T_{\text{reaction}} = 350$ °C, $P_{\text{total}} = 760$ Torr, and TOS = 0 min. The flow of PA varied from 0.03 to 0.3 mol/h. The catalyst was previously reduced under H_2 flow (100 mL/min) at 400 °C for 1 h for all cases.

pressure conditions using H₂ or H₂/He as a carrier gas. Catalyst particles were mixed with glass beads (Sigma Aldrich, 212–300 μ m) and packed between two layers of quartz wool inside a quartz reactor (0.25" OD). The reactor tube was placed in the center of a vertical furnace (Thermcraft Inc., 1200 W/115 V). All catalysts were pretreated in situ in hydrogen (100 SCCM) at 400 °C for 1 h. After reduction, the samples were cooled to the reaction temperature (300-400 °C). Pentanoic acid, mixed with heptane to prevent corrosion, was used as a feed. The reactants were injected using a syringe pump (KD Scientific) and vaporized (at 92-100 °C) before entering the reactor. The outlet stream was kept at 250 °C to prevent any product condensation. A gas chromatograph (GC), equipped with a flame ionization detector (FID) and an HP-INNOWAX column (Agilent, 60 m \times 0.32 mm ID \times 0.5 μ m), was connected to the reactor for product quantification. The same conditions mentioned above were used for experiments with the carbon nanotube samples, Pt/CNT/ MoO₃ and Pt/MoO₃/CNT.

2.4. Catalyst Characterization. *2.4.1. Scanning Electron Microscopy.* The samples were analyzed using a Thermo Quattro S field-emission environmental scanning electron microscope (FE-ESEM) with an accelerating voltage of 10 kV for imaging and 15 kV when performing energy-dispersive X-ray spectroscopy.

2.4.2. X-ray Photoelectron Spectroscopy. The AXIS-supra with a dual anode Al/Ag (2984.2 eV) monochromatic X-ray source was used to perform XPS analysis on the carbon nanotube samples.

2.4.3. Inductively Coupled Plasma Mass Spectrometry. A PerkinElmer NexION2000 inductively coupled plasma (ICP)-MS with laser ablation was used to analyze the Pt content on the synthesized CNT catalysts. The appropriate internal standards and dilution factors were selected based on a preliminary semiquantitative analysis. The samples were digested using the dry ashing method combined with acid extraction. Because multiwalled carbon nanotubes decompose above 500 °C, the catalyst samples (10–20 mg) were placed in a furnace at 700 °C for 2 h. The ashes from each sample were diluted with 2% HCl solution at room temperature and further diluted with ionized water before ICP-MS analysis.

3. RESULTS

3.1. Inhibition Effect of Pentanoic Acid. An inhibition effect is observed in the deoxygenation of PA over MoO₃ at a high partial pressure of PA (>3.0 Torr).¹⁹ To investigate whether this effect is also observed at a lower partial pressure of PA, the pressure was reduced (<3.0 Torr) at 350 °C, as shown in Figure 1a. Notably, reducing the partial pressure of PA changed the reaction order from inhibition (-0.24) to a zero-order (0th) regime with respect to PA. For 0.05 wt % Pt/MoO₃, the reaction order of PA shows a shift to zero-order dependence at a lower partial pressure of PA, as indicated in Figure 1b. This could lead to the interpretation that the surface is saturated with PA or that the rate is independent of PA at lower PA partial pressures. The mechanistic implications will be explained below.

To confirm that this zeroth order-dependence observed at low partial pressures of PA is not an artifact of the reaction products that are present at various conversion levels, the catalyst mass was decreased by 50%, and the rates were again measured at low partial pressures of PA (2.5 to 7.5 Torr). As a result, Figure S1 shows that the reaction rate is unchanged, while the conversion is reduced by 50%, as expected. Thus, these constant rates observed at a low PA partial pressure confirm the true zeroth order regime.

The reaction order with respect to PA was also investigated on the 0.05 wt % Pt/MoO₃ catalyst. Figure 1a,b indicates higher reaction rates for the conversion of PA over 0.05 wt % Pt/MoO₃ than MoO₃ under similar conditions. Although 0.05 wt % Pt/MoO₃ initially showed a higher conversion rate, this catalyst appears to be less resistant to inhibition by carboxylic acid. We hypothesize that this fast inhibition is due to the strong adsorption of the carboxylic acids onto the metal sites (Pt), rapidly decreasing the hydrogen coverage while hindering the regeneration of oxygen vacancies and conversion of PA. Thus, the catalyst surface of 0.05 wt % Pt/MoO₃ at high coverage of PA resembles the surface dynamics of MoO₃, where H₂ dissociation would likely be the rate-limiting step. In all cases, the rates were found by extrapolating to the initial time of stream (TOS) to eliminate the influence of catalyst deactivation.

The strong adsorption of PA over an oxygen vacancy might cause the inhibition effect observed at high partial pressures of PA over both MoO₃ and 0.05 wt % Pt/MoO₃. As previously reported, DFT calculations of the PA adsorption over MoO₃ indicate that the adsorption of PA through the carbonyl-group oxygen (C=O) at a defect site is 57 kJ/mol stronger than the adsorption through the hydroxyl group (-OH).¹⁹ Although the adsorption through the C=O group is stronger, the activation energy required to produce the aldehyde is significantly higher compared to the activation energy through the hydroxyl group, suggesting that the carboxylic acids adsorbed via the C=O group are only present as spectator species.¹⁹ Hence, we hypothesize that these strongly binding species are responsible for the inhibition behavior observed at 350 °C.

Consistent with this inhibiting behavior of acid is the increase in activation energy observed as the PA partial pressure increases. As shown in Figure 2, an increase in the

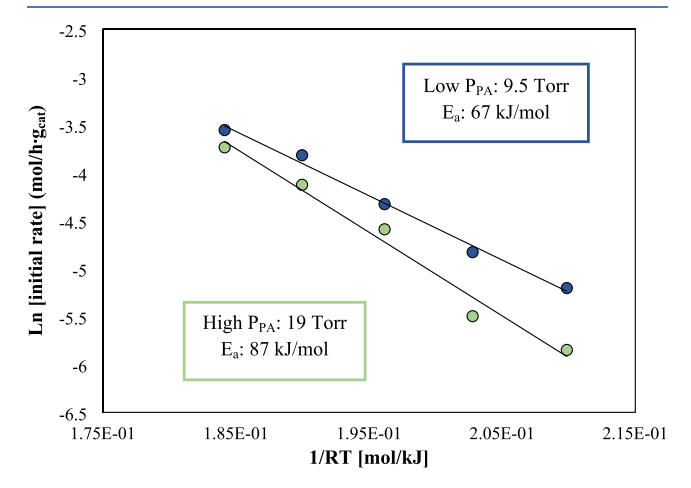


Figure 2. Activation energy comparison at a different partial pressure of PA over MoO₃. Reaction conditions: $P_{\text{total}} = 760$ Torr, Flow of H₂ = 30 mL/min, and TOS = 0 min. The catalyst was previously reduced under H₂ flow (100 mL/min) at 400 °C.

partial pressure of PA by a factor of 2 results in a 20 kJ/mol increase in the activation energy. This result supports the hypothesis that $\rm H_2$ dissociation is rate-limiting at a high partial pressure of PA due to the strong inhibition by PA. Previously, diminished activation barriers have been reported when comparing the $\rm Pt/MoO_3$ catalyst to $\rm MoO_3$ alone. ¹⁹ Comparing

the activation barrier for Pt/MoO₃ at higher partial pressures of acid co-fed reveals an identical activation barrier, as shown in Figure S2, indicating that the Pt sites still influence the chemistry at high PA partial pressures.

Figure 3 illustrates three possible explanations for the inhibition behavior observed at a high partial pressure of PA. Here, we hypothesize that the strong adsorption of carboxylic acids suppresses the surface reaction as one of the following:

- (i) Site competition over Pt metal sites between carboxylic acid (PA) and H₂ hinders H₂ dissociation.
- (ii) Site competition between PA and $\rm H_2$ on oxygen vacancies hinders $\rm H_2$ dissociation over these uncoordinated Mo species. 20
- (iii) Hindrance of hydrogen dissociation and spillover due to the high coverage of carboxylic acids.

For all three cases, H_2 dissociation and spillover are limited due to the high partial pressures of PA. Consequently, the limitations of hydrogen dissociation/spillover decrease the rate of formation and generation of oxygen vacancies, which explains the decrease in the rate of conversion of PA even in the presence of Pt clusters. In contrast, at lower coverage of PA, the surface reaction seems less limited by H_2 dissociation and spillover, as indicated by the shift in reaction order regime; more details will be discussed in Sections 3.2 and 3.5.

The selectivity toward pentanal is significantly affected by the concentrations of PA and hydrogen on the catalyst surface, particularly with regard to the 0.05 wt % Pt/MoO $_3$ catalyst. Figures S3 and S4 illustrate the selectivity profiles of both catalysts at 350 °C under low and high partial pressures of PA, respectively. At this temperature, it is anticipated that the presence of Pt as a promoter would lead to a reduction in selectivity toward PAL, as we have previously reported. ¹⁹ This reduction in selectivity can be attributed to the occurrence of side reactions facilitated by the presence of the Pt metal, leading to a shift in the overall selectivity. In contrast, as mentioned earlier, when MoO $_3$ is used alone as a catalyst, the selectivity toward PAL remains consistently high across all investigated partial pressures of PA.

When operating with a low partial pressure of PA over a 0.05 wt % Pt/MoO_3 catalyst, it is observed that the selectivity toward deoxygenated C-5 compounds decreases as the partial pressure of H_2 is reduced. Similarly, the production of the

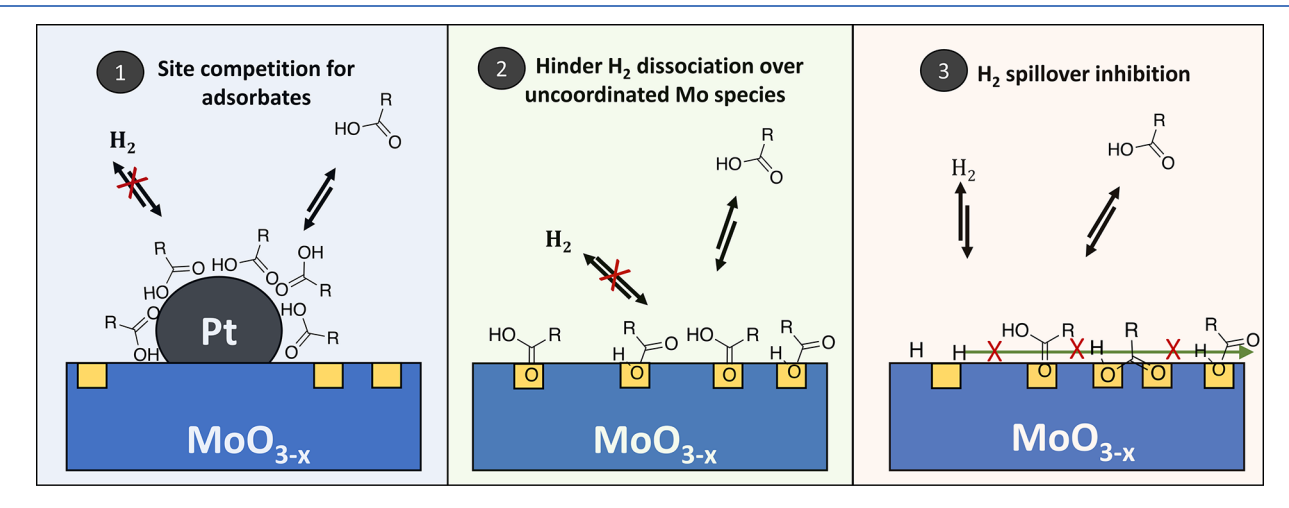


Figure 3. Possible causes of inhibition at a high partial pressure of PA: (i) Site competition for adsorbates over metallic Pt cluster on MoO_{3} , (ii) hindered H_2 dissociation at oxygen vacancies on MoO_{3} , and (iii) H_2 spillover inhibition on MoO_{3} .

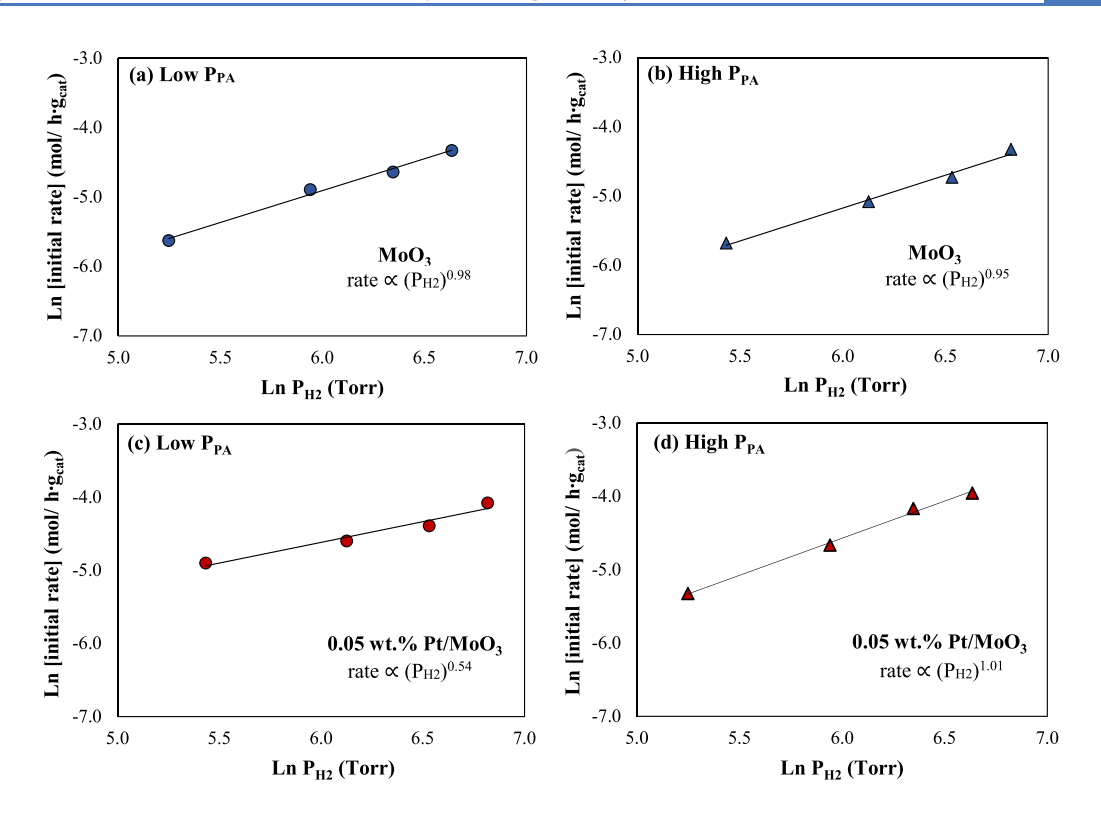


Figure 4. (a) Order of reaction with respect to H_2 using MoO_3 as a catalyst at low P_{PA} . (b) Order of reaction with respect to H_2 using MoO_3 as a catalyst at high P_{PA} . (c) Order of reaction with respect to H_2 over 0.05 wt % Pt/MoO_3 at low P_{PA} . (d) Order of reaction with respect to H_2 over 0.05 wt % Pt/MoO_3 at high P_{PA} . Reaction conditions: $P_{total} = 760$ Torr (H_2 pressure was varied and balanced with H_2 to maintain the same total pressure), $T_{reaction} = 350$ °C, and TOS = 0 min. Low $P_{PA} = 4.75$ Torr, and high $P_{PA} = 9.5$ Torr. The catalyst was previously reduced under H_2 flow (100 mL/min) at 400 °C for 1 h for all cases.

symmetrical ketone 5-nonanone increases as the $\rm H_2$ pressure is reduced. This reveals that under conditions such as these, where H addition to the adsorbed acid may be kinetically relevant, diminished H concentrations on the surface will modify the lifetime of adsorbed acid species and thus influence the concentration of adsorbed acid species on the surface. Longer lifetimes of adsorbed acids on the surface in the absence of nearby H atoms should result in an increased prevalence of acid-coupling reactions. Further, these longer lifetimes will diminish the concentration of available oxygen vacancies, thereby decreasing the probability of produced aldehydes from readsorbing on the catalyst surface and undergoing sequential deoxygenation chemistry to produce deoxygenated C-5 species. These results can be observed in Figure S3.

In contrast, at a moderate partial pressure of PA over 0.05 wt % Pt/MoO₃ catalysts, the selectivity toward pentanal decreases as hydrogen pressure decreases. Under these conditions, one may hypothesize that the high coverage of acid species hinders H_2 dissociation sufficiently such that it becomes the rate-determining step. Selectivity toward acid deoxygenation under these conditions decreases, while the formation of undesired C-4 compounds through decarbonylation/decarboxylation reactions over the metal sites decreases to a lesser extent, increasing product selectivity, as illustrated in Figure S4.

3.2. H₂ Effect on Reaction Order. Hydrogen plays an important role in HDO since it helps to form oxygen vacancies, enabling the catalyst surface to continually perform redox chemistry. To further investigate the kinetic relevance of hydrogen in this chemistry, the reaction order with respect to

 $\rm H_2$ was studied at both low and high partial pressures of PA for MoO₃ at 350 °C. Figure 4a,b shows that regardless of the partial pressure of PA, the reaction order with respect to $\rm H_2$ remains first-order. As shown in Figure S5, the same first-order dependence in $\rm H_2$ is observed at a lower temperature (320 °C).

Moreover, the reaction order with respect to H2 was also investigated over 0.05 wt % Pt/MoO3 catalyst. As shown in Figure 4c,d, we observed a change in the H₂ reaction order from 0.5 to 1.0 as the partial pressure of PA increased. This shift in the H₂ reaction order caused by the changes in the surface coverage of PA suggests that either hydrogen and PA compete for the same sites or that hydrogen is involved in the rate-limiting step. While catalysts deactivate as a function of time on stream, it is important to contrast the mechanistic implications from initial rate extrapolations from those observed during a longer time on stream. Figure S6 reveals that the shift in apparent reaction order holds for Pt/MoO₃ at low acid partial pressures when contrasted with MoO3 alone after 2.5 hours of reaction. Therefore, we hypothesize that at high partial pressures of PA, the surface dynamics of 0.05 wt % Pt/MoO₃ behaves similarly to MoO₃ since the strong inhibition effect of PA hinders the H₂ dissociation, as described above in Section 3.1.

3.3. Water Inhibition. Water is a by-product of oxygen vacancy formation. Similarly, the reverse reaction may also occur where water strongly adsorbs on an existing oxygen vacancy. Hence, the presence of water molecules occupying these sites can potentially impede the reaction rate of both catalysts. Similar observations were reported by Prasomsri et al.

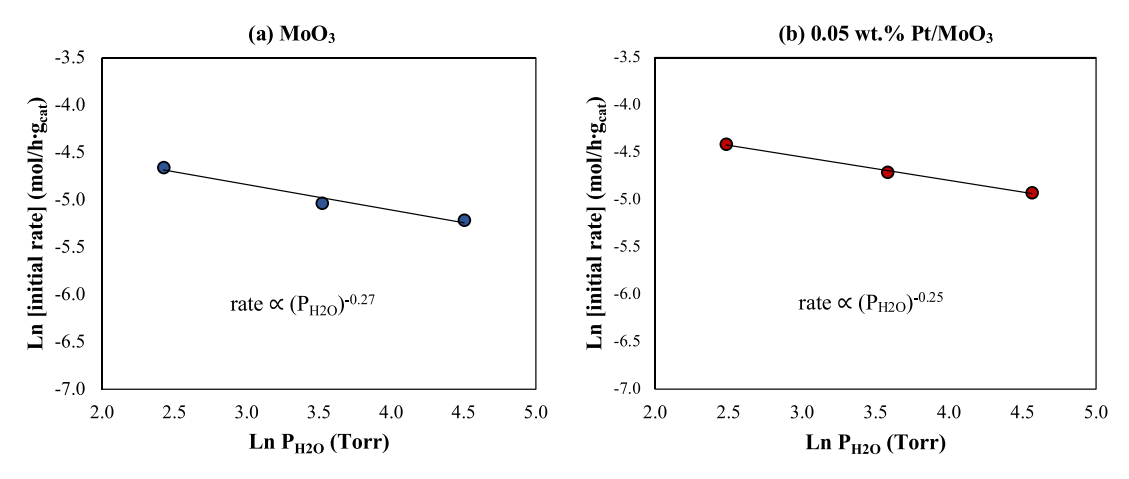


Figure 5. Dependence of reaction rate on the partial pressure of water over (a) MoO_3 and (b) 0.05 wt % Pt/MoO_3 . Reaction conditions: Flow of $H_2 = 30$ mL/min, $P_{total} = 760$ Torr, $T_{reaction} = 350$ °C, TOS = 0 min, and W/F = 0.11 g_{cat}/mL h. The catalyst was previously reduced under H_2 flow (100 mL/min) at 400 °C for 1 h for all cases.

in the conversion of acetone over MoO₃, where water was found to cause site blocking, negatively impacting the overall HDO activity without accelerating catalyst deactivation.¹⁶

In a detailed computational study, Head et al. investigated water interaction with MoO₃. Their study showed that water exhibits weak adsorption on a stoichiometric surface with an adsorption energy (E_{ads}) of -30 kJ/mol. However, when an oxygen vacancy is present on the surface, water shows stronger adsorption with an $E_{\rm ads}$ of -130 kJ/mol. Furthermore, it was observed that water could undergo dissociative adsorption on a surface featuring an oxygen vacancy, with an E_{ads} of -77 kJ/mol. They have also shown that dissociated water occurs on an O vacancy, forming two hydroxyl groups. However, these hydroxyl groups are less stable than the water molecule that is intact and adsorbed in an oxygen vacancy.³⁰ Therefore, the significant heat of adsorption exhibited by water over surface defects can potentially explain the inhibitory behavior observed when water is co-fed with acid, as depicted in Figure 5. A similar inhibiting effect is observed in both catalysts, MoO₃ and 0.05 wt % Pt/MoO₃.

The findings presented in this study differ significantly from other reported efforts for selective deoxygenation in the presence of water. First, the presence of water in the study conducted by Kammert et al. reveals enhanced rates of deoxygenated product formation, which the authors attribute to facilitated desorption of reactive intermediates. Similar behavior has been observed with other forms of deoxygenation chemistry when active metal-support interfacial sites are known to be kinetically relevant. We have revealed similar chemistry upon cresol deoxygenation upon water incorporation at a Ru-TiO2 interface, for example, where enhanced rates were attributed to proton-assisted C-O cleavage.³⁴ These events occurring either through Bronsted acid siteassisted cleavage or selective binding of reactive intermediates to interfacial sites lead to the rapid sequential conversion of aldehyde products to form alcohols and further products. Water incorporation in this case, both for MoO₃ and Pt/ MoO₃, reveals significant reductions in reaction rates, as shown in Figure 5, further emphasizing the important role of undercoordinated sites in this case without the necessity for direct binding to Pt metal sites to carry out deoxygenation chemistry. This further supports a distinct mechanism for acid deoxygenation chemistry from those reported in prior efforts.

3.4. Site Requirement for the Deoxygenation of Carboxylic Acids. Oxygen vacancies have been proposed as the active sites for the HDO of several biomass-derived compounds over MoO₃.¹⁷ Roman-Leshkov and co-workers have provided insights into the state of the surface during the deoxygenation of anisole over MoO₃ from NAP-XPS data, which indicate that the undercoordinated species are responsible for C–O bond activation.³¹ Their study suggests that Mo⁵⁺ species are active in this chemistry, while Mo⁴⁺ species do not seem to be involved in the deoxygenation of anisole.³²

To assess the importance of oxygen vacancies on the deoxygenation of PA to PAL, we used a micropulse reactor to study the initial interaction of reactants with the surface prior to surface modification (e.g., phase changes, overreduction, carbon deposition, and carboxylic acid saturation/inhibition). Figure S7 shows that pentanal formation is suppressed without the initial formation of oxygen vacancies formed during the reduction pretreatment. This was found to be the case even if hydrogen was added to each pulse. Thus, this confirms that the initial presence of oxygen vacancies formed during the reduction pretreatment prior to introducing PA is essential for the deoxygenation of PA.

Metal dopants are frequently incorporated to facilitate the formation of oxygen vacancies over metal oxides and increase rates. Using high-dispersion Ni metal deposition into MoO₃/ SiO2, Yang et al. showed an enhancement of m-cresol HDO selectivity. Their study suggests that the synergistic cooperation between Ni and MoO_x species is important to achieve high activity and selectivity.³³ Similar findings were reported by Rachmady et al. in the conversion of acetic acid in Pt/FeO₃, where the promoted catalyst showed improved activity and selectivity toward acetaldehyde. 12 However, the interaction of a reducible metal oxide with a hydrogen promoter metal can be complex due to the formation of multiple surface features that one might designate as active sites. 34,35 These prospective active sites can be categorized as short- and long-range interactions. Short-range interactions involve the active sites located in close proximity to the metal particle and its modifications around the interface. Long-range interactions, often referred to as promoter effects, are the active sites found on the support itself (surface defects, subsurface defects, or surface OH groups) that are created by the hydrogen spillover

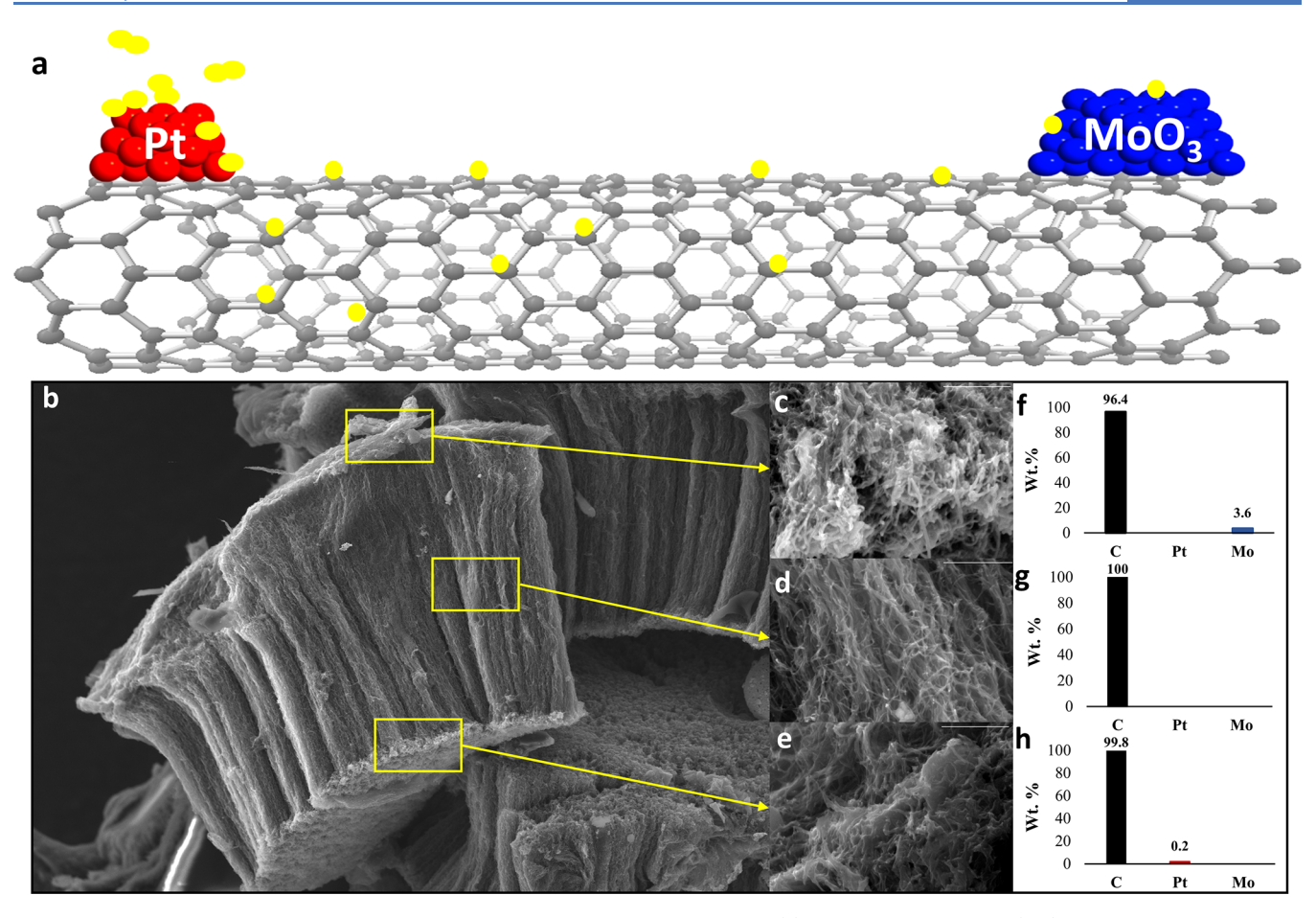


Figure 6. Carbon nanotube with metal and metal oxide deposited at opposite ends. (a) Illustration of a metal (red) capable of dissociating H_2 (yellow) onto a carbon nanotube where H atoms can travel across to a metal oxide (blue). (b) SEM image of a nanotube forest with Pt and MoO_3 deposited on opposite ends via metal evaporation. (c-e) Magnified portions of the top, middle, and bottom of the forest, respectively (scale bar indicates 1 μ m). (f-h) EDS results corresponding to the locations in (c) to (e).

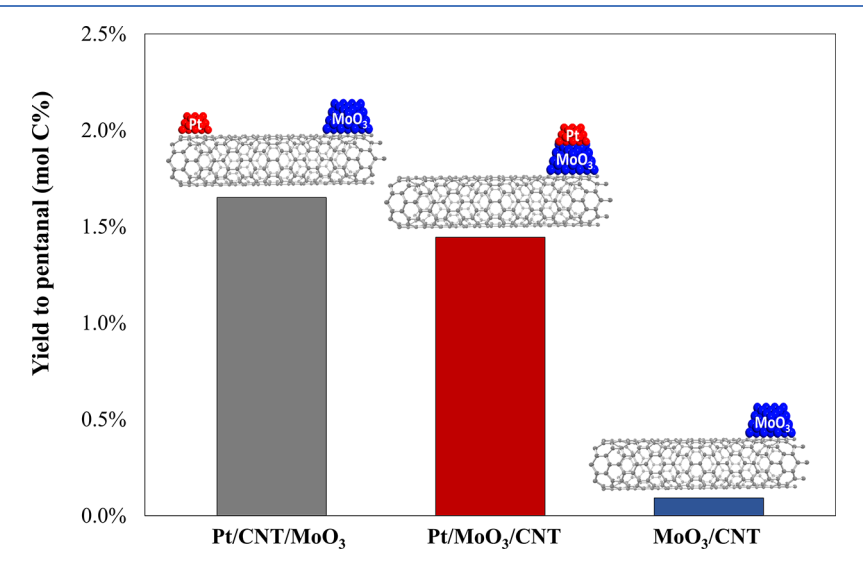


Figure 7. Pentanoic conversion over Pt and MoO₃ catalysts supported on CNTs. Reaction conditions: Flow of H₂ = 30 mL/min, P_{total} = 760 Torr, T_{reaction} = 330 °C, TOS = 0 min, and W/F = 0.3 g_{cat}/mL h. The catalyst was previously calcined in situ for 1 h at 400 °C and reduced under H₂ flow (100 mL/min) at 400 °C for 1 h.

from the hydrogen promoter metal to the reducible oxide support. ^{36,37}

To determine the role of Pt on MoO₃, a technique recently developed in our research group utilizes carbon nanotubes

(CNT) as hydrogen highways to evaluate the kinetic relevance of short- and long-range interactions. A similar approach has been used to discern the active site for the furfural conversion to methyl furan on Pd/TiO₂ and anisole deoxygenation on

Cu/TiO₂.²¹ To achieve this, Pt and MoO₃ were deposited on opposing ends of carbon nanotube forests of a controlled length. This allowed H atoms to migrate from Pt metal clusters to the MoO₃ surface and partially reduce the surface of MoO₃ without being in physical contact, as illustrated in Figure 6a.

The detailed synthesis preparation technique and characterization confirming their separation and their ability for hydrogen spillover is described in our published work²¹ and briefly discussed in the Experimental Section. Figure 6f-h shows EDS results along the nanotube forests with Pt and MoO₃ deposited on opposite ends, which confirms that Pt and MoO₃ are not in direct contact after reduction. Since a high loading of Pt can promote side reactions, the low ratio of Pt/ Mo was maintained for all these samples. The weight loadings of Mo were determined through a quartz crystal microbalance. Due to the low amount of Pt present among the CNTs, the weight loadings of Pt were determined with ICP-MS. Catalyst weight loadings can be found in Table S1. The oxidation states for these samples were evaluated via XPS in order to verify that the calcination process was sufficient to convert metallic Mo⁰⁺ into Mo⁶⁺. XPS results reported in Figure S8 indicate that the Mo species were fully oxidized after moderate calcination (400 °C) for 1 h.

Here, two different Pt/MoO₃ catalysts were prepared, one with the metals subsequently deposited on the same side of the nanotube forest (Pt/MoO₃/CNT) and another with the two catalytic materials deposited on the opposite ends of the nanotube forests (Pt/CNT/MoO₃). Figure 7 shows the results for the two catalysts in the deoxygenation of PA. As can be seen, there is no significant difference in the measured rates for the two catalysts. As these rates are very similar, we can infer that the role of Pt is to promote H₂ dissociation, leading to the formation of oxygen vacancies to sustain SDO activity over the catalyst surface. To further clarify the impact of incorporating Pt into MoO₃, we compared our findings for Pt/CNT/MoO₃ with the rate obtained when only MoO₃ is present on CNTs. The results indicate that MoO₃/CNT exhibits a significantly lower rate of pentanal production in the absence of Pt clusters. This can be attributed to the limited ability of MoO₃ to promote H₂ dissociation at 330 °C, thereby hindering the catalytic activity. Therefore, these results provide compelling evidence that Pt clusters are essential for facilitating hydrogen dissociation, thereby significantly enhancing catalytic activity and leading to noticeably higher reaction rates, as clearly illustrated in Figure 7.

To investigate the possibility of Pt and MoO₃ species coming into contact through sintering or Ostwald ripening during the reaction, SEM analysis was conducted on the spent catalyst. Figure S9 reveals that a small fraction of Mo species migrate across the CNTs during the reduction or reaction step. This indicates that a minor portion of Mo may be in direct contact with Pt species. However, the amount of interfacial area for the samples where Pt was introduced on opposing ends of the nanotube should be much lower than the sample where Pt was deposited directly on the MoO₃. Thus, this small fraction alone is highly unlikely to be responsible for the observed rate in Pt/CNT/MoO₃. Thus, we conclude that the sites at the metal/support interface are neither kinetically relevant nor responsible for the selective deoxygenation of PA to PAL when noble metals are incorporated at these low loadings; otherwise, the rate for SDO would be higher when Pt and MoO₃ are in direct contact. This technique confirms our hypothesis about the promoter effect of Pt clusters over MoO₃ on this chemistry.

3.5. Elementary Steps and Reaction Mechanism. It has been proposed that the deoxygenation of ketones and alcohols over MoO₃ occurs via a reverse Mars—van Krevelen mechanism, wherein an oxygen atom from the oxygenated compound is removed by an oxygen vacancy, re-establishing the initial surface structure.³⁸ Similar and related proposals have been made for other redox catalysts as well, with varying claims regarding the importance of co-fed hydrogen in the process. Thibodeau et al. have also proposed a closely related deoxygenation mechanism upon the conversion of acrolein over tungsten oxide bronzes.³⁹ A radical reverse Mars—van Krevelen mechanism type was proposed by Mironenko and Vlachos for the conversion of furfural to 2-methyl furan over Ru/RuO₂ using 2-propanol as both a solvent and hydrogen donor.²⁶

The deoxygenation of carboxylic acids over bifunctional catalysts has prompted the proposal of various mechanism types. Pestman et al. have observed that the conversion of acetic acid over Pt/TiO2 follows a Mars-van Krevelen mechanism. 13,40 In contrast, Rachmady and Vannice have explored the conversion of acetic acid to acetaldehyde using a Langmuir-Hinshelwood kinetic model, suggesting that active sites at the Pt/TiO2 interface play a crucial role in this reaction. 12,14 Similarly, Kammert et al. have investigated the conversion of propionic acid over Pd-ReOx-TiO2. Their findings indicate that Pd, serving as a metal promoter, facilitates H₂ dissociation, leading to the formation of surface hydrides essential for C-H bond formation. Furthermore, the acidic properties of the ReO_x-supported catalyst, particularly Bronsted sites, play a significant role in the dehydration process, leading to the production of propanal. Computational studies further highlight the importance of the proximity between Pd and ReO, which promotes the addition of hydride to the carbon of adsorbed species, forming diol-like intermediates. This intermediate further reacts with a surface proton and undergoes dehydration to produce propanal, which is readily hydrogenated to form propanol, given the importance of proximity to the Pd metal sites.⁴¹ However, as discussed above in Sections 3.3 and 3.4, the active sites for this catalyst involve undercoordinated Mo sites, not only interfacial sites, and the impact of water hinders rates at an initial time on stream, where deoxygenation rates are enhanced over the PdReO_x system, indicating distinct elementary steps for selective deoxygenation chemistry over the two catalysts.

Sections 3.1 and 3.2 show that the persistent presence of hydrogen on the catalyst surface is required to maintain high SDO rates. In this chemistry, hydrogen is typically involved in the formation/regeneration of oxygen vacancies and in the hydrogenation of PA to yield PAL. Our study suggests that complicating factors beyond a simplified MvK-type mechanism, such as the persistent surface coverage of neighboring dissociated H atoms, must be considered. Often, MvK-type mechanisms are modeled as Langmuir-Hinshelwood (LH)type mechanisms when additional complications such as those described above are present. 25,27 Utilizing a Langmuir-Hinshelwood framework, it is possible to account for the oxidant and reductant adsorption and dissociation on surface sites as well as adsorption competition with other reactants and products that could be present in the reaction mixture. 25,27 Although a MvK model can describe the redox chemistry at the surface of the MoO₃ catalyst, cases such as this one, where

local H coverage and site competition strongly influence reaction rates, are better approximated by a Langmuir-Hinshelwood (LH)-type modeling framework for the cases outlined here.

To develop a mathematical expression that describes the mechanism of the deoxygenation of PA, we will consider two different active sites, an oxygen vacancy, and a metallic active site. The active metal sites include undercoordinated Mo species created during the reduction process and Pt clusters present on the 0.05 wt % Pt/MoO₃ catalyst. No other active sites were considered since the presence of a significant kinetic contribution due to distinct active sites located in the metalsupport interface was ruled out.

The sequence of elementary steps proposed for this chemistry involves H₂ dissociation on the metal site [1], followed by H migration from metal sites to the MoO₃ surface [2]. When H spills over onto reducible oxides, it migrates as a proton/electron pair, following parallel but different paths.²⁴ Oxygen vacancy formation/regeneration is considered by combining two OH groups to yield one water molecule on the oxygen vacancy and an oxidized vacancy site, as described in step [3]. PA is assumed to adsorb dissociatively over metal sites and oxygen vacancies, as described in steps [4] and [5]. After PA is strongly adsorbed on an oxygen vacancy without H abstraction, as shown in step [6], 13 the adsorbed PA species undergoes the addition of one H atom [7]. These steps are highly dependent on H coverage. 19 To yield pentanal, the first hydrogenation is followed by a second H addition to the adsorbed species to produce pentanal in the gas phase and an adsorbed water molecule [8]. As described in steps [9] and [10], water and pentanal may compete for oxygen vacancies, modifying the surface coverage of kinetically relevant intermediates. The sequence of proposed elementary steps is described in Scheme 1. The apparent activation energy required for this chemistry is affected by both PA and H₂ partial pressure, as described above in Sections 3.1 and 3.2.

Several elementary steps were considered as potentially ratelimiting for this chemistry. The rate expression for each

Scheme 1. Proposed Elementary Steps for the Hydrogenation of PA over Promoted Pt/MoO₃^a

$$[1] H_{2(g)} + 2^{\bullet} \xrightarrow{K_{1}} 2H^{\bullet}$$

$$[2] H^{\bullet} + \Theta \xrightarrow{K_{2}} H^{\odot} + \bullet$$

$$[3] H^{\odot} + H^{\odot} \xrightarrow{K_{3}} H_{2}O^{\odot} + \Theta$$

$$[4] C_{4}H_{9}COOH_{(g)} + 2^{\bullet} \xrightarrow{K_{4}} C_{4}H_{9}COO^{\bullet} + H^{\bullet}$$

$$[5] C_{4}H_{9}COOH^{\odot} + \Theta \xrightarrow{K_{5}} C_{4}H_{9}COO^{\odot} + H^{\odot}$$

$$[6] C_{4}H_{9}COOH + \bigcirc \xrightarrow{K_{6}} C_{4}H_{9}COOH^{\odot}$$

$$[7] C_{4}H_{9}COOH^{\odot} + H^{\odot} \xrightarrow{K_{7}} C_{4}H_{9}COHOH^{\odot} + \Theta$$

$$[8] C_{4}H_{9}COHOH^{\odot} + H^{\odot} \xrightarrow{K_{8}} C_{4}H_{9}CHO + H_{2}O^{\odot} + \Theta$$

$$[9] H_{2}O^{\odot} \xrightarrow{K_{9}} H_{2}O(g) + \bigcirc$$

$$[10] C_{4}H_{9}CHO^{\odot} \xrightarrow{K_{10}} C_{5}H_{10}O_{(g)} + \bigcirc$$

^a(•) denotes the metal site, (⊙) denotes oxidized or healed oxygen vacancies, and (Ø) denotes reduced or empty oxygen vacancies. All rates are represented as quasi-equilibrated steps, which will be decoupled with varying hypothesized kinetically relevant steps below. possible rate-determining step considered for the deoxygenation of PA is shown in Table 1. Detailed mathematical

Table 1. Rate Expression for each Potential Rate-**Determined Step**

RDS	rate expression
H ₂ dissociation	$r_1 = k_1 P_{\mathrm{H2}}[\bullet]^2$
oxygen vacancy formation/regeneration	$r_3 = k_3 K_1 K_2^2 P_{\text{H2}} [\odot]^2$
first H addition to PA species	$r_7 = k_7 K_1^{0.5} K_6 K_2 P_{PA} P_{H2}^{0.5} [\emptyset] [\odot]$
second H addition to PA species	$r_8 = k_8 K_1 K_2^2 K_6 K_7 P_{\text{PA}} P_{\text{H2}} [\odot] [\varnothing]$

expressions for each case are shown in the Supplementary Information. In eqs 7 and 8, k_i is the intrinsic rate constant for the corresponding elementary step described in Scheme 1; K_i represents the equilibrium constant for step i; $[\varnothing]_0$ is the total number of oxygen vacancies; $[\bullet]_0$ is the total number of metallic sites available at the surface, and [⊙] are the oxidized oxygen vacancy sites, which are considered as a constant.

Here, $[\bullet]$ corresponds to metal balance sites. $[\bullet]_0$ represents the number density of all adsorption sites (vacant and occupied) on a catalyst surface.

$$[\bullet]_0 = [\bullet] + [H^{\bullet}] + [C_4 H_9 COO^{\bullet}]$$
 (1)

$$[\bullet] = \frac{[\bullet]_0}{(1 + K_1^{1/2} P_{H2}^{1/2} + K_4 P_{PA} / K_1^{1/2} P_{H2}^{1/2})}$$
(2)

The expression for $[\emptyset]$ can be obtained by site balance of the oxygen vacancies as follows:

$$\begin{split} [\varnothing]_0 &= [\varnothing] + [C_4 H_9 COO^{\varnothing}] + [C_4 H_9 COOH^{\varnothing}] \\ &+ [C_4 H_9 COHOH^{\varnothing}] + [H_2 O^{\varnothing}] + [C_4 H_9 CHO^{\varnothing}] \end{split} \tag{3}$$

Since [C₄H₉COOH^Ø] is the only significant surface intermediate species on the oxygen vacancies, the following expression gives a balance of [ø] sites:

$$[\varnothing]_0 = [\varnothing] + [C_4 H_9 COOH^{\varnothing}] \tag{4}$$

 $\left[C_4H_9COOH^{\varnothing}\right]$ is obtained by the adsorption constant related to step 5:

$$[\varnothing]_0 = [\varnothing] + K_6 P_{PA}[\varnothing]$$
 (5)

$$[\varnothing] = \frac{[\varnothing]_0}{(1 + K_6 P_{PA})} \tag{6}$$

In a computational study, Shetty et al. reported that H₂ dissociation shows the highest barrier for the overall reaction in the HDO of acetone to propylene over a pristine MoO₃ catalyst (164 kJ/mol). Typically, H2 dissociation takes place through a homolytic bond breaking without prior surface activation, which explains this high barrier value for H2 dissociation on MoO₃. 42 Although a real catalyst contains defects (including oxygen vacancies) at the catalyst surface that can lower the activation energy for H2 dissociation, the deoxygenation of PA on MoO3 could still be limited by this step. In fact, the rate expression depicted in eq 7 was determined by considering H₂ dissociation as the rate-limiting step (RDS1, step 1), which shows a first-order dependence on H₂ pressure, consistent with the experimental results for MoO₃ in Figure 4a,b. Here, we consider other potential ratedetermining steps in addition to H₂ dissociation that also exhibit a first-order dependence with respect to H₂ pressure,

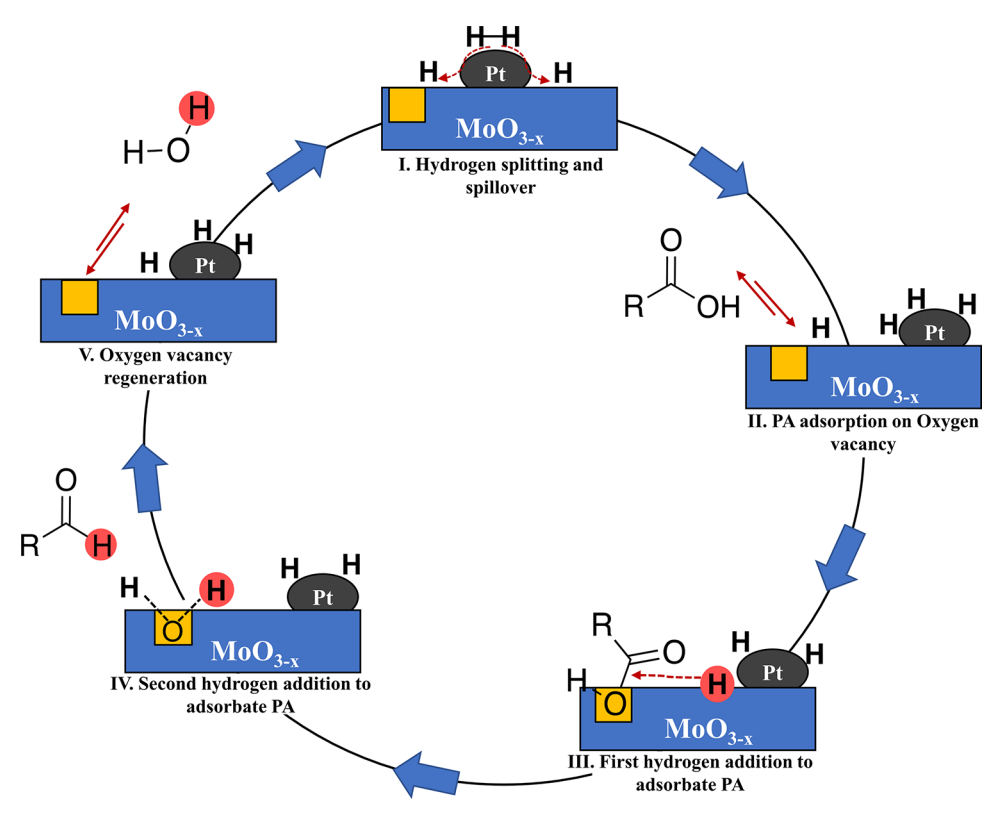


Figure 8. Proposed mechanism for the deoxygenation of carboxylic acid over Pt/MoO₃.

such as oxygen vacancy formation, which we have previously indicated as a possibility, 19 or the second H atom addition to the adsorbed PA species, as shown in Table 1. Due to the strong dependence of this reaction on the persistent presence of hydrogen on the catalyst surface, and not simply defects, we had previously speculated that H addition to the carbonyl carbon could be an important rate-determining step over promoted Mo catalysts. We had also proposed that vacancy creation may be important for unpromoted catalysts. However, the reaction order suggests that the prior step of H₂ dissociation is the more likely the RDS over-unpromoted MoO₃ catalyst and over-promoted Pt/MoO₃ catalysts at high acid partial pressures. The lack of kinetic relevance associated with the formation of oxygen vacancies over MoO₃ lies in DFT calculations that suggest that once the H atoms form, they can diffuse over the surface easily (\sim 38–60 kJ/mol) and form an oxygen vacancy with a total activation energy of 22 kJ/mol, 42 which is far lower than the barriers we observed experimentally.

$$r_{1} = \frac{k_{1} P_{H2}[\bullet]_{0}}{(1 + K_{1}^{1/2} P_{H2}^{1/2} + K_{3} P_{PA} / K_{1}^{1/2} P_{H2}^{1/2})^{2}}$$
(7)

Since the presence of the Pt cluster promotes H_2 dissociation, a different rate-limiting step is considered for 0.05 wt % Pt/MoO₃. Figure 4c shows that the reaction order with respect to H_2 is between 0.5 and 0.6. Two rate-determining steps could result in a 0.5 dependence on hydrogen: the addition of the first H atom to the adsorbed PA species or hydrogen spillover on MoO₃, according to Table 1. As H_2 is dissociative over the Pt cluster, H atoms tend to form -OH groups at the surface with low energy barriers (\sim 38–60 kJ/mol), ⁴² favoring hydrogen spillover along the MoO₃ surface. In Section 3.4, we show that hydrogen spillover

is not likely to be the rate-determining step of this reaction since Pt/MoO_3 that are in direct contact $(Pt/MoO_3/CNT)$ show similar rates as Pt/MoO_3 separated by carbon nanotubes $(Pt/CNT/MoO_3)$. Therefore, the rate expression described by eq 8 assumes that the H addition to an adsorbed PA is the rate-limiting step (RDS2, step 7). Our experimental results are in agreement with the experimental data at low partial pressures of PA for 0.05 wt % Pt/MoO_3 shown in Figure 4c. Thus, the presence of Pt in this catalyst serves as a source for accelerating hydrogen activation to maintain the constant hydrogen supply at the surface, lowering the energy barrier and enhancing the rate of conversion of PA, as described in Section 3.2. Rachmady et al. have shown similar H_2 dependence on the hydrogenation of acetic acid at the interfacial sites of Pt/TiO_2 .

$$r_7 = \frac{k_7 K_1^{1/2} K_6 K_2 P_{PA} P_{H2}^{1/2} [\odot]_0 [\varnothing]_0}{(1 + K_6 P_{PA})}$$
(8)

Our experimental results reveal that upon the incorporation of Pt, the reaction order with respect to H₂ shifted from 1 to 0.5 at a low partial pressure of PA, as shown in Figure 4a,c. This change in reaction order is due to the change in hydrogen coverage at the surface. Therefore, this reaction is highly dependent on the local hydrogen concentration since more H atoms will participate in the hydrogenation of the carboxylic acid. Furthermore, the incorporation of Pt clusters on MoO₃ not only increases rates of H₂ dissociation but may also facilitate the formation of hydrogen bronzes (H_xMoO₃), which are H species that diffuse into the support and intercalate into the structure by forming -OH bonds with the oxide. The formation of these hydrogen bronzes on 0.05 wt % Pt/MoO₃ could contribute to maintaining the local hydrogen concentration at the surface, enhancing hydrogenation reactions.

Kosydar et al. have also reported that Pt/H_xMoO_3 showed higher selectivity towards C=O hydrogenation in the conversion of cinnamaldehyde and furfural. This is also in agreement with the selective hydrogenation of acrolein to allyl alcohol, where Pt/H_xMoO_3 can easily activate aldehyde oxygen atoms and promote hydrogen addition.

Overall, the kinetic model framework presented here demonstrates that a Langmuir-Hinshelwood-type reaction mechanism describes the deoxygenation of PA over promoted Pt/MoO₃, with orders matching those observed experimentally. As the concentration of PA increases over the catalyst, the results suggest that the RDS shifts from r7 at low PA concentrations in the presence of a metal capable of maintaining a high H coverage on the surface. At high concentrations of PA, the RDS shifts to r1, with a negative order-dependence on increasing PA at significant PA coverages. This suggests that the concentration of PA not only influences hydrogen coverage but also modifies the RDS. Figure 8 shows the mechanism proposed for the deoxygenation of carboxylic acid over promoted Pt/MoO₃. A similar mechanism has previously been used to explain the hydrogenation of acetic acid in the interfacial region of Pt/TiO_{2.} although in that case, spillover to carry out this chemistry on O vacancies far from the Pt metal particle is unlikely, as we propose in the current study. 12,14

4. CONCLUSIONS

The mechanistic details of pentanoic acid conversion on promoted Pt/MoO₃ give evidence that the deoxygenation of PA takes place primarily at the metal oxide surface (i.e., on oxygen vacancies) rather than on highly active sites located at the interface, which is ruled out by an experiment using carbon nanotubes as hydrogen bridges between the two catalytic functionalities (Pt and MoO_x). Our results suggest that the role of Pt is to maintain a high hydrogen concentration at the surface. This study shows that a Langmuir-Hinshelwood-type mechanism can describe the conversion of pentanoic acid over both MoO₃ and 0.05 wt % Pt/MoO₃, assuming two types of active sites: metal sites that activate H2 and oxygen vacancies that enable the deoxygenation of PA. The RDS of the reaction shifts with the partial pressure of acid and H2 coverage from H addition to the adsorbed acid species to H₂ dissociation. Overall, this study provides a mechanistic understanding of the deoxygenation of PA on dynamic MoO3 catalysts in the presence and absence of small amounts of metal promoters.

ASSOCIATED CONTENT

Supporting Information

The Supporting Information is available free of charge at https://pubs.acs.org/doi/10.1021/acscatal.3c01053.

Weight percentage of all deposited metals on Pt/CN/MoO₃ and Pt/MoO₃/CNT; order of reaction with respect to pentanoic acid over MoO₃ at different masses of catalyst; activation energy at high partial pressure of pentanoic acid over 0.05 wt % Pt/MoO₃; product selectivity distribution at low and high pentanoic acid partial pressures and varying H₂ partial pressures over MoO₃ and 0.05 wt % Pt/MoO₃ catalysts; reaction order with respect to PA over MoO₃ at 320 °C; pentanoic acid conversion rate over MoO₃ and Pt/MoO₃ at a low partial pressure of pentanoic acid; conversion of PA over MoO₃ without H₂ pretreatment; XPS results for calcined

MoO₃/CNT, MoO₃, and MoO₂; binding energies of Mo 3d doublet for Mo⁴⁺, Mo⁵⁺, and Mo⁶⁺ as determined by XPS characterization; proposed sequence of elementary steps and derived rate expression (PDF)

AUTHOR INFORMATION

Corresponding Author

Steven P. Crossley — School of Chemical, Biological, and Materials Engineering, University of Oklahoma, Norman, Oklahoma 73019, United States; orcid.org/0000-0002-1017-9839; Email: stevencrossley@ou.edu

Authors

- Laura A. Gomez School of Chemical, Biological, and Materials Engineering, University of Oklahoma, Norman, Oklahoma 73019, United States
- Caleb Q. Bavlnka School of Chemical, Biological, and Materials Engineering, University of Oklahoma, Norman, Oklahoma 73019, United States
- Tianhao E. Zhang School of Chemical, Biological, and Materials Engineering, University of Oklahoma, Norman, Oklahoma 73019, United States
- Daniel E. Resasco School of Chemical, Biological, and Materials Engineering, University of Oklahoma, Norman, Oklahoma 73019, United States; orcid.org/0000-0001-5342-0621

Complete contact information is available at: https://pubs.acs.org/10.1021/acscatal.3c01053

Notes

The authors declare no competing financial interest.

ACKNOWLEDGMENTS

This work has been supported by the National Science Foundation (grant no. 1653935), whose support is gratefully acknowledged. XPS analysis was performed using instrumentation funded in part by the National Science Foundation Major Research Instrumentation Program under grant no. CHE-1338173.

REFERENCES

- (1) Huber, G. W.; Iborra, S.; Corma, A. Synthesis of Transportation Fuels from Biomass: Chemistry, Catalysts, and Engineering. *Chem. Rev.* **2006**, *106*, 4044–4098.
- (2) Chheda, J. N.; Huber, G. W.; Dumesic, J. A. Liquid-Phase Catalytic Processing of Biomass-Derived Oxygenated Hydrocarbons to Fuels and Chemicals. *Angew. Chem., Int. Ed.* **2007**, *46*, 7164–7183.
- (3) Li, C.; Zhao, X.; Wang, A.; Huber, G. W.; Zhang, T. Catalytic Transformation of Lignin for the Production of Chemicals and Fuels. *Chem. Rev.* **2015**, 11559.
- (4) Zhang, M.; Yao, R.; Jiang, H.; Li, G.; Chen, Y. Insights into the Mechanism of Acetic Acid Hydrogenation to Ethanol on Cu(111) Surface. *Appl. Surf. Sci.* **2017**, *412*, 342–349.
- (5) Pei, Z.-F.; Ponec, V. On the Intermediates of the Acetic Acid Reactions on Oxides: An IR Study. *Appl. Surf. Sci.* **1996**, *103*, 171–182.
- (6) Bond, J. Q.; Martin Alonso, D.; West, R. M.; Dumesic, J. A. γ-Valerolactone Ring-Opening and Decarboxylation over SiO2/Al2O3 in the Presence of Water. *Langmuir* **2010**, *26*, 16291–16298.
- (7) Bond, J. Q.; Alonso, D. M.; Wang, D.; West, R. M.; Dumesic, J. A. Integrated Catalytic Conversion of Gamma-Valerolactone to Liquid Alkenes for Transportation Fuels. *Science* **2010**, 327, 1110–1114.

- (8) Wright, W. R. H.; Palkovits, R. Development of Heterogeneous Catalysts for the Conversion of Levulinic Acid to γ -Valerolactone. *ChemSusChem* **2012**, *5*, 1657–1667.
- (9) Chiappero, M.; Do, P. T. M.; Crossley, S.; Lobban, L. L.; Resasco, D. E. Direct Conversion of Triglycerides to Olefins and Paraffins over Noble Metal Supported Catalysts. *Fuel* **2011**, *90*, 1155–1165.
- (10) Yadav, V.; Sivakumar, G.; Gupta, V.; Balaraman, E. Recent Advances in Liquid Organic Hydrogen Carriers: An Alcohol-Based Hydrogen Economy. *ACS Catal.* **2021**, 14712.
- (11) Singh, A. K.; Singh, S.; Kumar, A. Hydrogen Energy Future with Formic Acid: A Renewable Chemical Hydrogen Storage System. *Catal. Sci. Technol.* **2016**, 12.
- (12) Rachmady, W.; Vannice, M. A. Acetic Acid Hydrogenation over Supported Platinum Catalysts. *J. Catal.* **2000**, *192*, 322.
- (13) Pestman, R.; Koster, R. M.; Pieterse, J. A. Z.; Ponec, V. Reactions of Carboxylic Acids on Oxides: 1. Selective Hydrogenation of Acetic Acid to Acetaldehyde. *J. Catal.* 1997, 168, 255–264.
- (14) Rachmady, W.; Vannice, M. A. Acetic Acid Reduction by H2 over Supported Pt Catalysts: A DRIFTS and TPD/TPR Study. *J. Catal.* **2002**, 207, 317–330.
- (15) He, Z.; Wang, X. Hydrocarbon Production from Carboxylic Acids via Catalytic Deoxygenation: Required Catalytic Properties. *ACS Symp. Ser.* **2013**, *1132*, 301.
- (16) Prasomsri, T.; Nimmanwudipong, T.; Román-Leshkov, Y. Effective Hydrodeoxygenation of Biomass-Derived Oxygenates into Unsaturated Hydrocarbons by MoO3 Using Low H2 Pressures. *Energy Environ. Sci.* **2013**, *6*, 1732–1738.
- (17) Prasomsri, T.; Shetty, M.; Murugappan, K.; Román-Leshkov, Y. Insights into the Catalytic Activity and Surface Modification of MoO3 during the Hydrodeoxygenation of Lignin-Derived Model Compounds into Aromatic Hydrocarbons under Low Hydrogen Pressures. *Energy Environ. Sci.* **2014**, *7*, 2660–2669.
- (18) Shetty, M.; Murugappan, K.; Prasomsri, T.; Green, W.; Roman-Leshkov, Y. Reactivity and Stability Investigation of Supported Molybdenum Oxide Catalysts for the Hydrodeoxygenation (HDO) of m-Cresol. *J. Catal.* **2015**, *331*, 86–97.
- (19) Gomez, L. A.; Bababrik, R.; Komarneni, M. R.; Marlowe, J.; Salavati-fard, T.; D'Amico, A. D.; Wang, B.; Christopher, P.; Crossley, S. P. Selective Reduction of Carboxylic Acids to Aldehydes with Promoted MoO3 Catalysts. *ACS Catal.* **2022**, *12*, 6313–6324.
- (20) Shetty, M.; Buesser, B.; Román-Leshkov, Y.; Green, W. H. Computational Investigation on Hydrodeoxygenation (HDO) of Acetone to Propylene on α -MoO3 (010) Surface. *J. Phys. Chem. C* **2017**, *121*, 17848–17855.
- (21) Briggs, N. M.; Barrett, L.; Wegener, E. C.; Herrera, L. V.; Gomez, L. A.; Miller, J. T.; Crossley, S. P. Identification of Active Sites on Supported Metal Catalysts with Carbon Nanotube Hydrogen Highways. *Nat. Commun.* **2018**, *9*, 3827.
- (22) Omotoso, T.; Herrera, L. V.; Vann, T.; Briggs, N. M.; Gomez, L. A.; Barrett, L.; Jones, D.; Pham, T.; Wang, B.; Crossley, S. P. Stabilization of Furanics to Cyclic Ketone Building Blocks in the Vapor Phase. *Appl Catal B* **2019**, 254, 491.
- (23) Abreu Teles, C.; Duong, N.; Rabelo-Neto, R. C.; Resasco, D.; Noronha, F. B. Evidence of Dependence between the Deoxygenation Activity and Metal—Support Interface. *Catal. Sci. Technol.* **2022**, *12*, 5961—5969.
- (24) Prins, R. Hydrogen Spillover. Facts and Fiction. Chem. Rev. **2012**, 112, 2714–2738.
- (25) Vannice, M. A. An Analysis of the Mars-van Krevelen Rate Expression. *Catal. Today* **2007**, *123*, 18.
- (26) Mironenko, A. V.; Vlachos, D. G. Conjugation-Driven "Reverse Mars-van Krevelen"-Type Radical Mechanism for Low-Temperature C-O Bond Activation. *J. Am. Chem. Soc.* **2016**, *138*, 8104.
- (27) Doornkamp, C.; Ponec, V. The Universal Character of the Mars and Van Krevelen Mechanism. *J. Mol. Catal. A: Chem.* **2000**, 162, 19.
- (28) Pestman, R.; Duijne, A.; Pieterse, J.; Ponec, V. The Formation of Ketones and Aldehydes from Carboxylic Acids, Structure-Activity

- Relationship for Two Competitive Reactions. J. Mol. Catal. A 1995, 103, 175–180.
- (29) de Mattos, J. C. P.; Rodrigues, L. F.; de Moraes Flores, É. M.; Krivan, V. Determination of Trace Impurities in Aluminum Nitride by Direct Solid Sampling Graphite Furnace Atomic Absorption Spectrometry. Spectrochim Acta Part B At Spectrosc 2011, 66, 637—643
- (30) Head, A. R.; Gattinoni, C.; Trotochaud, L.; Yu, Y.; Karslloğlu, O.; Pletincx, S.; Eichhorn, B.; Bluhm, H. Water (Non-)Interaction with MoO3. *J. Phys. Chem. C* **2019**, *123* (), DOI: 10.1021/acs.jpcc.9b03822.
- (31) Polo-Garzon, F.; Blum, T. F.; Bao, Z.; Wang, K.; Fung, V.; Huang, Z.; Bickel, E. E.; Jiang, D. E.; Chi, M.; Wu, Z. In Situ Strong Metal-Support Interaction (SMSI) Affects Catalytic Alcohol Conversion. ACS Catal. 2021, 11, 1938–1945.
- (32) Murugappan, K.; Anderson, E.; Teschner, D.; Jones, T.; Skorupska, K.; Roman-Leshkov, Y. Operando NAP-XPS Unveils Differences in MoO3 and Mo2C during Hydrodeoxygenation. *Nat. Catal.* **2018**, *1*, 960.
- (33) Yang, F.; Libretto, N. J.; Komarneni, M. R.; Zhou, W.; Miller, J. T.; Zhu, X.; Resasco, D. E. Enhancement of M-Cresol Hydrodeoxygenation Selectivity on Ni Catalysts by Surface Decoration of MoOx Species. ACS Catal. 2019, 9, 7791.
- (34) Omotoso, T. O.; Baek, B.; Grabow, L. C.; Crossley, S. P. Experimental and First-Principles Evidence for Interfacial Activity of Ru/TiO2 for the Direct Conversion of m-Cresol to Toluene. *ChemCatChem* **2017**, 9 (), DOI: 10.1002/cctc.201700157.
- (35) Cargnello, M.; Doan-Nguyen, V. V. T.; Gordon, T. R.; Diaz, R. E.; Stach, E. A.; Gorte, R. J.; Fornasiero, P.; Murray, C. B. Control of Metal Nanocrystal Size Reveals Metal-Support Interface Role for Ceria Catalysts. *Science* **2013**, *341*, 771.
- (36) Komaya, T.; Bell, A. T.; Weng-Sieh, Z.; Gronsky, R.; Engelke, F.; King, T. S.; Pruski, M. Effects of Dispersion and Metal-Metal Oxide Interactions on Fischer-Tropsch Synthesis over Ru/TiO2 and TiO2-Promoted Ru/SiO2. *J. Catal.* **1994**, *150*, 400.
- (37) Resasco, D. E.; Haller, G. L. A Model of Metal-Oxide Support Interaction for Rh on TiO2. *J. Catal.* **1983**, *82*, 279.
- (38) Mars, P.; van Krevelen, D. W. Oxidations Carried out by Means of Vanadium Oxide Catalysts. *Chem. Eng. Sci.* **1954**, *3*, 41.
- (39) Thibodeau, T. J.; Canney, A. S.; Desisto, W. J.; Wheeler, M. C.; Amar, F. G.; Frederick, B. G. Composition of Tungsten Oxide Bronzes Active for Hydrodeoxygenation. *Appl Catal A Gen* **2010**, 388, 86
- (40) Grootendorst, E. J.; Pestman, R.; Koster, R. M.; Ponec, V. Selective Reduction of Acetic Acid to Acetaldehyde on Iron Oxides. *J. Catal.* **1994**, *148*, 261–269.
- (41) Kammert, J. D.; Chemburkar, A.; Miyake, N.; Neurock, M.; Davis, R. J. Reaction Kinetics and Mechanism for the Catalytic Reduction of Propionic Acid over Supported ReO XPromoted by Pd. ACS Catal. 2021, 11, 1435.
- (42) Rellán-Piñeiro, M.; López, N. A Coupled Density Functional Theory-Microkinetic Modeling for the Hydrodeoxygenation of Glycerol to Propylene on MoO3. ACS Sustainable Chem. Eng. 2018, 6, 16169.
- (43) Noh, H.; Wang, D.; Luo, S.; Flanagan, T. B.; Balasubramaniam, R.; Sakamoto, Y. Hydrogen Bronze Formation within Pd/MoO3 Composites. *J. Phys. Chem. B* **2004**, *108* (), DOI: 10.1021/jp0307506.
- (44) Kosydar, R.; Kołodziej, M.; Lalik, E.; Gurgul, J.; Mordarski, G.; Drelinkiewicz, A. The Role of Hydrogen Bronzes in the Hydrogenation of Polyfunctional Reagents: Cinnamaldehyde, Furfural and S-Hydroxymethylfurfural over Pd/HxWO3 and Pd/HxMOO3 Catalysts. *Int. J. Hydrogen Energy* **2022**, *47* (), DOI: 10.1016/j.ijhydene.2021.10.162.
- (45) Hoang-Van, C.; Zegaoui, O. Studies of High Surface Area Pt/MoO3 and Pt/WO3 Catalysts for Selective Hydrogenation Reactions. II. Reactions of Acrolein and Allyl Alcohol. *Appl. Catal. A Gen.* **1997**, 164 (), DOI: 10.1016/S0926-860X(97)00160-9.